DOI: 10.1002/fuce.201800034

Synthesis of Graphitic Mesoporous Carbon from Metal Impregnated Sili Template for Proton Exchange Membrane Fuel Cell Application

ORIGINALRESEARCHPAPER

K. N. Sultana[1], D. Worku[1], M. T. Z. Hossain[2], S. Ilias[2]*

[1] Department of Nanoengineering, Joint School of Nanoscience & Nanoengineering, North Carolina A & T State University, Greensboro, NC 27411, USA

[2] Department of Chemical, Biological and Bioengineering, North Carolina A & T State University, Greensboro, NC 27411, USA

Received March 14, 2018; accepted January 06, 2019; published online ¢¢¢

Abstract

High surface area graphitic mesoporous carbons (M-mGMC; M=Ni, Fe, Co or Ni-Fe) were synthesized via catalytic graphitization using a hard template based synthesis method. In house prepared SBA-15 silica material was impregnated with metal precursors to obtain M/SBA-15, template for M-mGMC synthesis. These materials were studied using different material characterization techniques, such as nitrogen adsorption desorption (BET), X-ray diffraction (XRD) analysis, Raman spectroscopy, X-ray photoelectron spectroscopy (XPS), Thermogravimetric analysis (TGA) and differential scanning calorimetry (DSC). Specific surface area ranging from 1,227.9 $m^2 g^{-1}$ to 1,320.7 $m^2 g^{-1}$ was observed for four M-mGMCs. Raman spectroscopy, XPS and wide angle XRD suggested presence of graphitic structure in these materials along with disorders. Electrocatalytic performance of these materials along with conventional carbon black (Vulcan XC-72) were evaluated in a single-stack proton exchange membrane fuel cell (PEMFC). Pt/NiFe-mGMC exhibited enhanced electrocatalytic activity compared to Pt/Ni-mGMC, Pt/Fe-mGMC and Pt/Co-mGMC electrocatalysts. However, Pt/NiFe-mGMC lacked adequate proton transport in membrane electrode assembly (MEA) compared to Pt/Vulcan XC-72. This exploratory study showed that NiFe-mGMC may find application as electrocatalyst support material in PEMFC.

Keywords: Carbon, Catalytic Graphitization, Electrocatalyst, Fuel Cell, Mesoporous Materials, OMC, Photoelectron Spectroscopy, Raman Spectroscopy, SBA-15, X-ray Diffraction

1 Introduction

Proton exchange membrane fuel cell (PEMFC) has attracted attention for energy application, due to its high energy density, low temperature operation and rapid start-up feature. Despite many advantages, large-scale commercialization of PEMFC remains a challenge, due to the high cost of platinum (Pt), which is the catalyst of choice. To protect the Pt-electrocatalyst from CO poisoning, high-purity hydrogen as fuel in PEMFC is a necessity. In hydrogen fuel, CO as impurity as low as 10.0 ppm can deactivate the Pt-catalyst [1]. Pt-catalyst is supported on conventional activated carbon (carbon black), which is susceptible to corrosion in fuel cell environment. This results in electrocatalyst degradation and loss of active Pt surface area [2, 3].

Characteristics of catalyst support play an important role in attaining stability and high dispersion of Pt metal particles. The desired properties of electrocatalyst support are: (i) large surface area to allow Pt metal dispersion across the surface of support material, (ii) good electrical conductivity to increase the electrochemical activity, and (iii) large accessible pores to enhance the reactant transport [4]. Carbon black has an irregular structure, which is mostly microporous (<2.0 nm). In membrane electrode assembly (MEA), the Pt metal particles deposited in micropores may have limited

access to electrocatalysis (due to increased diffusional resistance), leading to low Pt uti-

PAPER

[*] Corresponding author, ilias@ncat.edu

lization [5]. Catalyst support material with high specific surface area and mesopores (2.0 nm to 50.0 nm) is crucial for uniform dispersion of Pt-catalyst loading. Ordered mesoporous carbon (OMC), which has high specific surface area (>1,000 $m^2 g^{-1}$) and hexagonal mesopores, offers promising application in PEMFC as catalyst support [3]. However, OMC's amorphous structure leads to limited electrical conductivity, which deteriorates fuel cell performance [6, 7]. Recent study by Nettelroth et al. suggested that graphitization is required for high electrocatalytic activity of mesoporous carbon [8]. In addition, graphitized carbon supports have relatively small number of edge plane sites responsible for carbon oxidation; which provides more resistance to corrosion than carbon black at fuel cell operating conditions. Partially covalent bond in Pt-C arising from electron delocalization between Pt d orbital and abundant p sites of graphitized carbon supposedly helps to inhibit Pt oxidation and dissolution at intermediate potential during fuel cell operation [9].

Graphitic carbon materials can be obtained by high temperature treatment (>2,500 C) of carbon precursors [10]. Also at low temperature (<1,000 C), catalytic graphitization in the presence of transition metals have been reported [11–15]. However, high temperature graphitization involves consumption of high energy and results in significant structural shrinkage. Catalytic graphitization using transition metals (Ni, Fe, Co, Mn, etc.) is advantageous over high temperature graphitization in terms of time of preparation and graphitization conditions [16–18]. In recent years, there has been growing interest in catalytic graphitization to retain the porous structure in the resultant carbon [10, 12, 19]. Effect of iron oxide catalyst on catalytic graphitization of OMC at 700 C was studied by Nettelroth et al. and reported improved graphitic structure of the carbon [8]. Huang et al. used a dual-template method to synthesize well-crystallized graphitic carbon; however the surface area was found to be relatively low (326.0 $m^2 g^{-1}$) compared to OMC [20]. Tang et al. reported the catalytic graphitization of OMC at 700 C in the presence of transition metal oxides [21]. Although ordered mesostructure was retained, specific surface area (ranging from 525.0 $m^2 g^{-1}$ to 572 $m^2 g^{-1}$) of the resultant carbons were not comparable to that of pure OMC.

Graphitic mesoporous carbons with porous structure were obtained by our research group via catalytic graphitization using transition metals (M = Ni, Fe and Co) using M-SBA-15 as template [22]. Transition metal oxides were responsible for graphitizing mesoporous carbons. These M-OMC materials preserved high specific surface area with short range-order and partially graphitic structure.

In this paper, we present a hard template based technique to synthesize graphitic mesoporous carbon by employing transition metals for catalytic graphitization. Catalytic graphitization of the carbon was carried out in the presence of Ni, Fe, Co and Ni-Fe combination which has not been reported in the literature. Instead of using the one-pot synthesis of metal containing silica template, in this study, impregnation of SBA-15 material with metal salts used in a later step, followed by the reduction to investigate their catalytic effect on graphitization.

These metal precursors were used to graphitize OMC at relatively low temperature, as pure OMC failed to exhibit desired electron transport property due to its amorphous nature despite having high surface area. Four different templates obtained by impregnating SBA-15 mesoporous silica with transition metals (M/SBA-15; M = Ni, Fe, Co or Ni-Fe) were used as template to synthesize metal modified graphitic mesoporous carbons (M-mGMC). In this paper, we report the material characteristics of M-mGMCs and their performance in PEMFC.

2 Experimental

2.1 Materials and Methods

Analytical grade chemicals were used in this work. Ethanol, acetone, isopropanol, TEOS (tetraethyl orthosilicate, 98.0%), sucrose (99.0%), ammonium hydroxide, sulfuric acid (98.0%), $CoCl_26H2O$ (Cobalt chloride hexahydrate), $H_2PtCl_66H_2O$ (hydrogen hexachloroplatinate hexahydrate), HF (hydrofluoric acid, 48.0 – 50.0%) were obtained from Fisher Scientific, New Jersey, USA. Pluronic P123, HCl (ACS reagent, 37.0%) and $Fe(NO_3)_39H_2O$ (iron nitrate nonahydrate) were purchased from Sigma Aldrich, Missouri, USA. $Ni(NO_3)_26H_2O$ (nickel nitrate hexahydrate) was purchased from Alfa Aesar, Massachusetts, USA. Carbon Black Vulcan XC-72 and Nafion membrane (NRE212-30) were procured from Fuel Cell Earth LLC, Massachusetts, USA. CTAB (cetyltrimethylammoniumbromide, +99%) was purchased from Acros Organics, New Jersey, USA.

2.2 M-mGMC Synthesis Procedure

Figure 1 illustrates the various steps used to synthesize M-mGMCs and subsequent catalysts starting with SBA-15. SBA-15 was prepared following the procedure described by Zhao et al. [23] (Figure 1a). Then SBA-15 was impregnated with precursors of Ni, Fe and Co to prepare four M/SBA-15 templates (M = Ni, Fe, Co or Ni-Fe). $Ni(NO_3)_26H_2O$, $Fe(NO_3)_39H_2O$ and $CoCl_26H_2O$ were used as precursors for Ni, Fe and Co, respectively (Figure 1b). The molar ratio of different components used in the synthesis of SBA-15 was TEOS: CTAB: P123: H_2O: HCl: Ethanol = 1.0: 0.08: 0.02: 41.0: 5.90: 7.50. TEOS was used as silica precursor and CTAB was used as water phase surfactant during SBA-15 synthesis. The quantities of transition metal precursors used for impregnation of SBA-15 material were based on the total metal loading requirement of 10.0 wt.% in the final M/SBA-15. Metal precursor was dissolved in ethanol followed by addition of SBA-15. This mixture was stirred and dried at 60.0 C for 6 h, which was subsequently calcined at 500 C for 6 h. The calcined material was reduced at 600 C for 6 h under hydrogen flow to obtain M/SBA-15 template. For Ni-Fe/SBA-15, precursor salt of Ni and Fe (weight ratio of Ni:Fe in template is 1:1) was dissolved together in ethanol and abovementioned steps were carried out to obtain the final template.

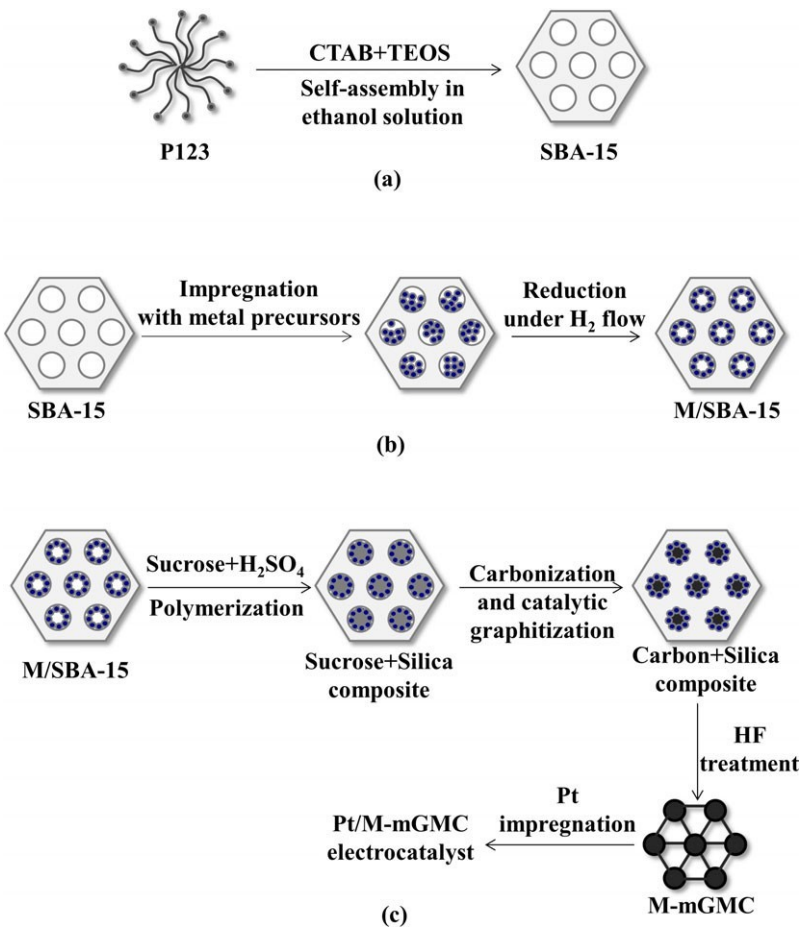

Fig. 1 Schematic of synthesis procedure for (a) SBA-15, (b) M/SBA-15 materials, (c) M-mGMC materials and electrocatalysts.

In M-mGMC materials synthesis step, sucrose was used as the carbon precursor (Figure 1c). Sucrose solution was prepared, which contained 1.25 g of sucrose, 5.0 mL of deionized (DI) water and 0.076 mL of H_2SO_4. Subsequently, M/SBA-15 template was added to sucrose solution. The resulting mixture was heated in a tube furnace for 6 h at 100 C, and another 6 h at 160 C. Second solution was prepared by dissolving 0.8 g sucrose and 0.049 mL H_2SO_4 in 5.0 mL DI water; to which, silica sample containing partially polymerized sucrose from previous step was added. Two-step heating procedure was repeated to dry the resulting mixture. The dried sample was carbonized at 900 C for 6 h under N_2 flow and cooled down to room temperature. After carbonization, the material was treated with aqueous hydrofluoric acid solution (5.0 wt.% HF) for 5 h followed by washing with DI water. The template-free carbon was dried overnight at room temperature followed by drying at 120 C for 8 h.

2.3 Electrocatalyst and Membrane Electrode Assembly (MEA) Preparation

Electrocatalysts for PEMFC were prepared by impregnating OMC, M-mGMCs and commercially available carbon tribution black (Vulcan XC-72) with $H_2PtCl_66H_2O$ dissolved in acetone. The amount of Pt precursor salt used is based on the Pt metal content of 20.0 wt.% in the final electrocatalyst. To reduce $PtCl_6^{2-}$ ions to platinum, impregnated OMC, M-mOMC and Vulcan XC-72 were treated under hydrogen flow at 350 C for 2 h. Nafion membrane was employed in the membrane electrode assembly. The catalyst ink for the MEA was prepared by adding Nafion ionomer to reduced catalyst dissolved in isopropanol. The quantity of Nafion ionomer in Pt/ Pt/Vulcan XC-72 was adjusted based on 33.0 wt.% Nafion in catalyst layer with platinum loading of 0.4 mg cm^{-2}. MEA was prepared by spraying the ink onto both sides of 5.0 cm^2 Nafion membrane.

2.4 Materials Characterization

Surface area measurement and pore size analysis of the OMC and M-mGMC materials were performed using a Quantachrome NOVA 2200e surface area and pore size analyzer (Quantachrome Instruments, Florida, USA). Specific surface area was calculated from the adsorption branch of the isotherm by applying the Brunauer-Emmett-Teller (BET) equation for a range of relative pressure, p/p_o (total pressure/vapor pressure) from 0.07 to 0.3 [24]. The pore size dis(PSD) was calculated using DFT method. X-ray diffraction (XRD) analysis of

M-mGMCs was performed using D8 DISCOVER X-ray diffractometer (Bruker Optics, Inc., Billerica, MA). The X-ray diffractometer was operated at 40.0 kVand 40.0 mA and diffraction patterns were recorded using CuKa radiation (wavelength of 1.5406 Å) in the range of 20.0–70.0 2q angle. XploRA One Raman Confocal Microscope System (Horiba Scientific, Kyoto, Japan) was used to record Raman spectra of M-mGMC materials where 532 nm laser was used as the excitation source. The X-ray photoelectronic spectroscopy (XPS) was carried out using a Hemispherical Energy Analyzer PHOIBOS 150 (SPECS Surface Nano Analysis GmbH, Berlin, Germany) with Mg Ka (1,254.0 eV) source. TGA-DSC analysis was carried out to investigate the decomposition behavior and residual metal content of the M-mGMCs using a SDT Q600 V20.4 Build 14 system (TA Instruments, Delaware, USA). Airflow of 100.0 mL min^{-1} was maintained inside the chamber during the analysis and M-mGMC samples were heated up to 1,000 C with temperature ramping of 10.0 C min^{-1}. Performance of synthesized Pt/OMC and Pt/M-mGMC electrocatalysts were evaluated in a Model 850e Compact Fuel Cell Test System (Scribner Associates, North Carolina, USA) by observing cell polarization. Pure hydrogen (anode) and air (cathode) was supplied to the single stack fuel cell at flow rates of

1.2 L min^{-1} and 2.5 L min^{-1}, respectively, under atmospheric pressure. Polarization test was carried out for 5.0 cm^2 MEA at 70.0 C by scanning current with a current density increment of 20.0 mA cm^{-2} per minute until the cell voltage dropped to ~0.02 V.

PAPER

3 Results and Discussions

3.1 N_2 Adsorption-desorption Isotherms

Adsorption-desorption isotherms of the OMC and M-mGMC materials are shown in Figure 2. These materials showed Type H1 hysteresis loop (typically found in materials with narrow range of uniform mesopores) and type IV isotherm according to IUPAC classifications, which is typical characteristic of mesoporous materials [25]. Three welldefined regions can be identified in these isotherms, which is in agreement with published results by Zhao et al. [23]. A closer inspection of the isotherms indicates weak adsorption on the mesopore walls at relative pressure ratio, $p/p_o <$ 0.4. Capillary condensation was observed in the relative pressure range of 0.4~0.9 due to progressive filling of the mesopores. Saturation level is attained at relative pressure, $p/p_o > 0.9$, which is indicative of complete pore filling. This is a typical feature of type IV isotherm [25].

Pore size distribution of the synthesized OMC and M-mGMC samples are shown in Figure 3, while in Table 1, BET surface area, pore size and pore volume of these materials are summarized. BET surface area of these materials was found to be ranging from 1,151 to 1,360 m^2g^{-1} with maximum uncertainty of + 45.90 m^2g^{-1}. Most of the pores of M-mGMC ranged in a narrow band of 4.0 nm to 6.0 nm. Synthesized M-mGMCs had higher specific surface area and larger pore size compared to OMC (Table 1). Increased specific surface area is attributed to the formation of graphene scaffold like structure on the wall of the M-mGMCs, which is discussed in XPS analysis section (Section 3.4). This is due to catalytic effect

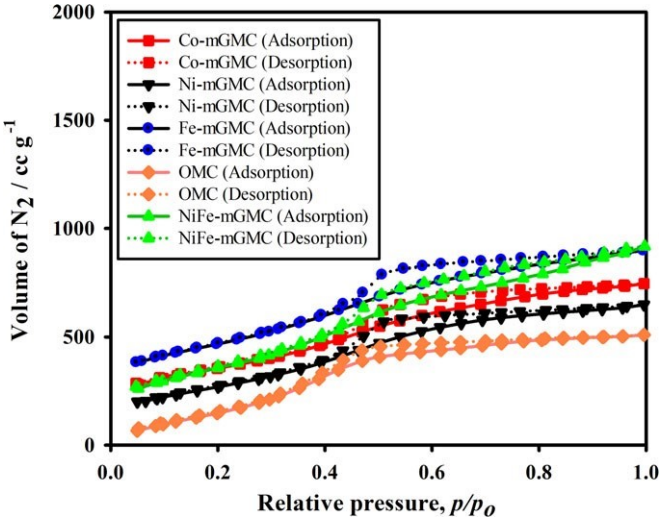

Fig. 2 N_2 adsorption desorption isotherm for synthesized OMC and M-mGMCs.

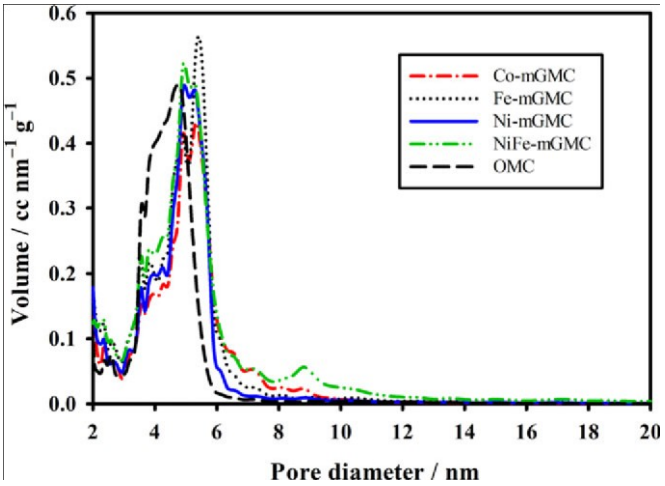

Fig. 3 Pore size distribution for synthesized OMC and M-mGMCs.

Table 1 Specific surface area, pore size and pore volume of OMC and M-mGMCs.

Material type	Specific surface area / m_2 g_{-1}	Average pore size / nm	Average pore volume / cc g^{-1}
NiFe-mGMC	1,359.6 + 45.90	4.3	1.4
Ni-mGMC	1,260.6 + 32.65	3.7	1.1
Fe-mGMC	1,343.1 + 22.43	3.7	1.2
Co-mGMC	1,267.5 + 28.75	3.7	1.2
OMC	1,151.3 + 31.13	3.4	1.1

of the transition metals during carbonization. The larger pore sizes of M-mGMCs compared to OMC may be due to the presence of transition metals in pore walls of M/SBA-15 (silica template) that results in formation of smaller diameter carbon rods. Upon removal of M/SBA-15 silica template with 5.0 wt.% HF solution, larger pores of M-mGMCs were obtained. These enhanced properties of the materials provide better Pt metal dispersion and improved mass transfer of the reactants.

3.2 X-ray Diffraction Analysis

Wide angle x-ray diffraction pattern of M-mGMCs (Fe, Ni, NiFe, and Co-mGMC) are presented in Figure 4. Well-resolved peaks are observed at ~23.0 and ~43.0 for M-mGMC materials, which corresponds to parallel arrays in (002) and (100) crystalline, planes, respectively. These two planes are indexed for graphene as suggested by Zhang et al. [26]. These peaks are attributed to characteristics of graphene revealing the presence of two dimensional hexagonally arranged carbon atoms in M-mGMCs [26]. Nonetheless, the low intensity of the peaks indicates low degree of graphitization in these materials. Among all M-mGMCs, Ni-mGMC has the sharpest peak at

~43.0, which suggests higher degree of graphitization during carbonization of the material resulting from better catalytic effect by Ni than Co or Fe. At 23.0 2q angle NiFe-mGMC

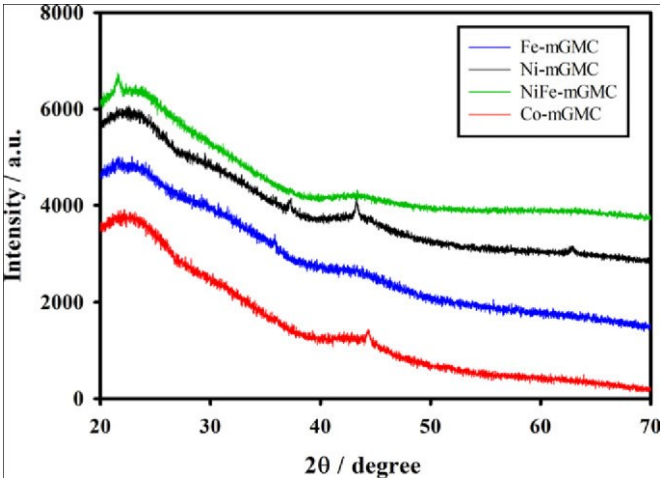

Fig. 4 X-ray diffraction pattern for M-mGMC materials.

showed the sharpest peak, which indicates that NiFe bimetal combination is better catalyst for graphitization of OMC than Ni, Co or Fe.

3.3 Raman Spectroscopy

Raman spectra for M-mGMC materials are shown in Figure 5. In these materials, we observed two bands at ~1,333 cm^{-1} and ~1,582 cm^{-1} known as D and G band, respectively. D band is associated with the C–C single bonds between sp^3 hybridized carbon atoms, which indicates the presence of defects in the graphite layer [27, 28]. G band corresponds to in-plane displacement of the sp^2 bonded carbons due to Raman scattering. Higher energy of sp^2 bonds compared to sp^3 bonds drives the vibrational frequency corresponding to graphitic carbon bonds to higher frequency. G band at 1,582 cm^{-1} depicts the presence of sp^2 bonds in synthesized M-mGMC indicating graphitic structure of these materials. These observations are consistent with the structural characteristics found from XRD patterns of these materi-

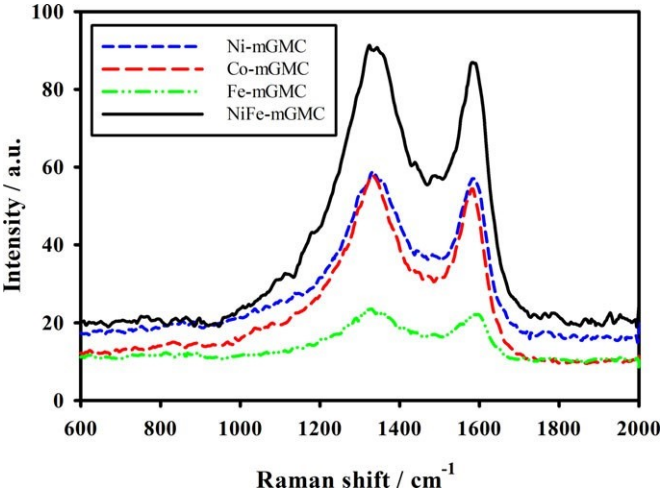

als. ID/IG ratio for Ni-, Co-, Fe- and NiFe-mGMCs was calculated as 1.039, 1.056, 1.068 and 1.065, respectively, whereas 1.001 was the corresponding value reported for OMC [22]. These ID/IG ratios suggest, though synthesized M-mGMCs contain graphitic structure, they have disorder in graphitic layers resulting in higher intensity of D-band compared to G-band [27].

3.4 X-ray Photoelectron Spectroscopy (XPS)

Typical XPS spectra of (a) Ni-mGMC, (b) Co-mGMC, (c) Fe-mGMC, (d) NiFe-mGMC, and (e) OM

Figure 6. Carbon 1s spectra of these materials are deconvoluted into three peaks with binding energies of 284.4, 285.6 and 286.6 eV which may be attributed to sp^2, sp^3 and possibly either due to sp^2 plasmon or C–O bond, respectively [29]. In OMC and M-mGMC materials, atomic percentage of oxygen varied from 2.7 to 4.4% and could be responsible for C-O bond. We observed variations in the ratio of sp^2 and sp^3 concentration for different transition metals used in graphitization. Although all M-mGMCs showed high concentration of sp^2 bonded carbon, which is indicative of presence of graphene like scaffold in these materials. We observed highest sp^2 concentration in NiFe-mGMC (Figure 6d) among all M-mGMCs, as indicated in Table 2. This could be attributed to the synergistic effect of Ni and Fe for catalytic graphitization during carbonization [30]. Due to higher sp^3 concentration present in Fe-mGMC compared to other mGMCs (Table 2), the material showed less graphitic characteristics. This analysis is also in agreement with the Raman spectroscopy (Figure 5) where the highest ID/IG ratio was observed for Fe-mGMC. XPS analysis suggested that Ni-, Co- and NiFe-mGMC contains higher concentration of sp^2, i.e., higher graphitization degree than OMC.

3.5 Thermogravimetric Analysis and Differential Scanning Calorimetry (TGA-DSC)

Thermal decomposition of M-mGMC materials were investigated using TGA and DSC (Figure 7). From TGA, three welldistinct regions for weight loss of these materials can be identified in the temperature range of 20–480 C, 480–620 C and >620 C. We observed slight weight loss in the range of 20–480 C, which was mainly due to the loss of moisture. Sig-

Fig. 5 Raman spectra for M-mGMC materials.

Table 2 Relative concentrations of sp^2 and sp^3 bonded carbon in OMC and M-mGMC materials.

Material type	sp^2 concentration / %	sp^3 concentration / %	sp^2 to sp^3 concentration ratio
Fe-mGMC	79.12	20.88	3.79
Ni-mGMC	85.71	14.29	6.00
Co-mGMC	84.09	15.91	5.29
NiFe-mGMC	87.50	12.50	7.00
OMC	83.33	16.67	5.00

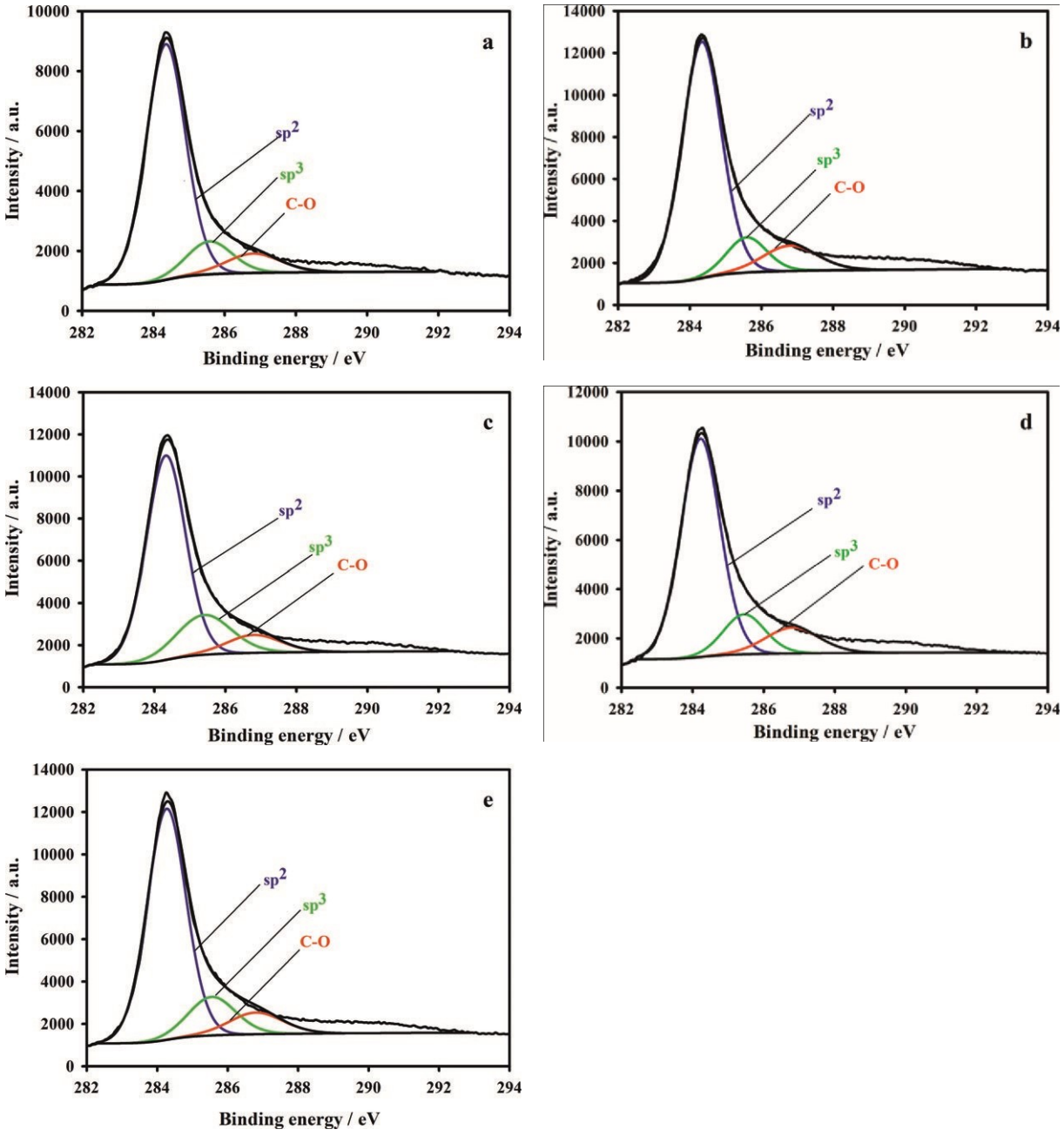

Fig. 6 Deconvoluted C1s spectra of: (a) Ni-mGMC, (b) Co-mGMC, (c) Fe-mGMC, (d) NiFe-mGMC, and (e) OMC from x-ray photoelectron spectroscopy.

nificant loss of weight due to the oxidation of carbon was observed at temperature range of 480–620 C for M-mGMCs. We observed slightly different decomposition behavior of Fe-mGMC from the rest of the materials. This may be due to the oxidation states of Fe and their decomposition during thermal analysis; the instability of iron oxide at temperature below 575 C results in its breakdown and formation of other oxides (different oxidation state). At temperature above 620 C, no further weight loss was observed and the metal residue was found to be in the range of 2.0–4.0 wt.%.

3.6 Fuel Cell Tests

Performance of the Pt/M-mGMCs, Pt/OMC and Pt-Vulcan XC-72 electrocatalysts during fuel cell polarization test is shown in Figure 8. In the ohmic polarization region, Pt/NiFemGMC materials demonstrated higher current density when compared with Pt/Ni-mGMC, Pt/Fe-mGMC, Pt/Co-mGMC, and Pt/OMC (Figure 8a). For example, at cell potential of 0.4 V, highest current density among M-mGMCs was observed for Pt/NiFe-mGMC (420.0 mA cm^{-2}), which was much higher compared to Pt/OMC (80.0 mA cm^{-2}). However, higher compared to that of Pt/OMC (33.11 mW cm^{-2}), Pt/Ni-mGMC (123.58 mW cm^{-2}), Pt/Co-mGMC (55.9 mW cm^{-2}) and Pt/Fe-mGMC (110.5 mW cm^{-2}). Fuel cell tests suggest that Ni-Fe could be the choice of catalyst for graphitization of mesoporous carbon.

compared to OMC may be accounted for improved electrocatalytic activity in concentration polarization

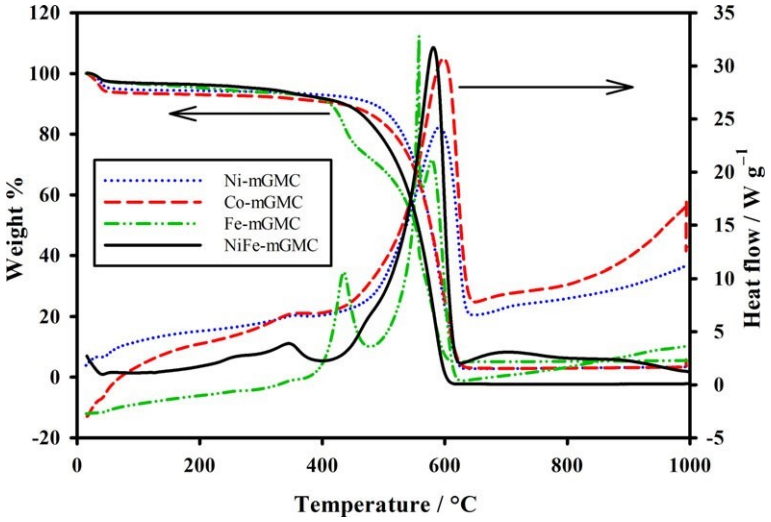

Pt/Vulcan Fig. 7 TGA-DSC plots for synthesized M-mGMCs.

XC-72 performed better in the ohmic polarization region compared to other electrocatalysts. Inferior performance of Pt/OMC is attributed to amorphous nature of OMC. Higher current density of Pt/NiFe-mGMC among all M-mGMCs could be attributed to the significant catalytic effect of Ni-Fe bimetal during graphitization, which performs better than Ni or Fe, as discussed in XPS analysis section (see Section 3.4). The degree of formation of graphene like scaffolds in NiFemGMC is higher compared to rest of the M-mGMCs, which resulted in smaller electrical resistance of Pt/NiFe-mGMC. This also explains the significant improvement of performance in concentration polarization region during fuel cell test (see Section 3.2). Pt/Ni-mGMC performed better than Pt/FemGMC and Pt/Co-mGMC, which may be attributed to the better catalytic effect of Ni than Fe or Co [12]. Reactant transport into the pores of NiFe-mGMC along with electron transport property of the material improved due to better catalytic effect, which greatly affected the cell polarization. However, relatively poor performance of NiFe-mGMC compared to Vulcan XC-72 may be attributed to mass transfer limitations in the pores. Small pore size of M-mGMCs could be a rate limiting factor for proton transport, due to limited accessibility of Nafion ionomer inside the pores. For Vulcan XC-72, Pt deposition mostly takes place on the outer surface and the interface between Pt and Nafion allows effective proton transport in the membrane electrode assembly [31]. Figure 8b shows power density curves for synthesized electrocatalysts. The maximum power density obtained for Pt/NiFe-mGMC was found to be 168.34 mW cm^{-2}, which is much

4 Conclusion

In summary, graphitized mesoporous carbons (M-mGMC) with high specific surface area were synthesized via catalytic graphitization using Ni, Co, Fe and Ni-Fe combination. M/SBA-15, obtained by impregnating with these transition metals, was used as the sacrificial hard template for M-mGMC synthesis. These M-mGMC materials had high specific surface area, mesopores, partially graphitic structure and large pore volume that are highly desirable characteristics of catalyst support materials for fuel cell applicat ORIGINALRESEARCHPAPER of these materials is attributed to the formation of graphene like sp^2 bonds between carbon atoms of M-mGMCs as confirmed by Raman spectroscopy and wide angle XRD studies. Larger pore size of M-mGMCs

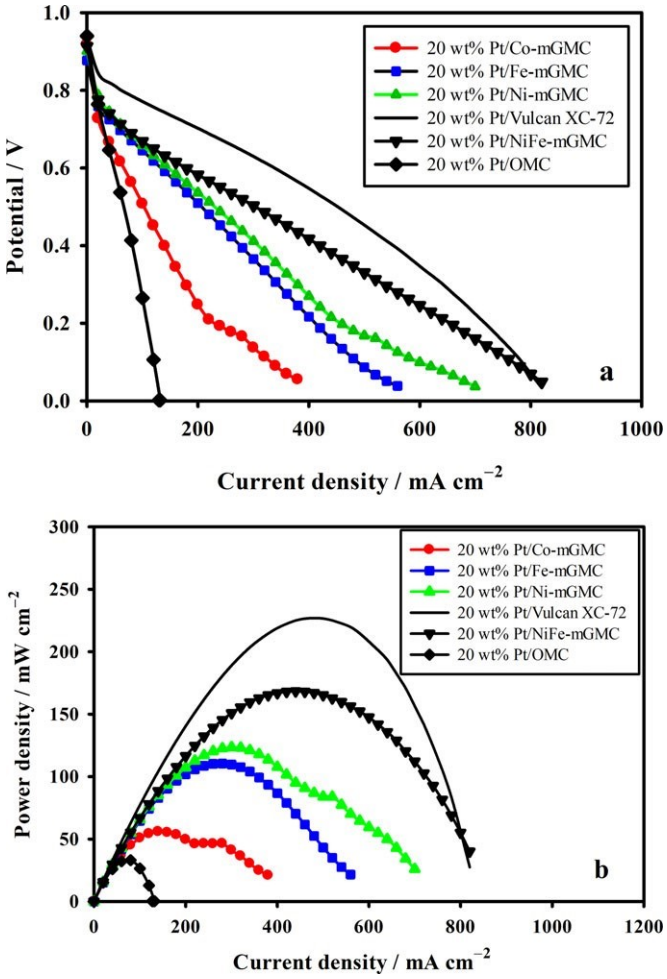

Fig. 8 (a) Polarization curves, and (b) power density curves for synthesized electrocatalysts.

region. This study showed that NiFe-mGMC as electrocatalyst support material may have a promise in PEMFC application. Synergistic catalytic effect of Ni-Fe combination is accountable for enhanced electron transport property of NiFe-mGMC, which decreased the ohmic loss and resulted in high power density in Pt/NiFe-mGMC electrocatalyst based cell stack. If the mass transfer limitation issue could be adequately addressed, NiFe-mGMC that has favorable surface area, may find application in developing low Pt-loading electrocatalyst for PEMFC.

Acknowledgements

The authors would like to acknowledge support of this research from National Science Foundation through NSF CREST Bioenergy Center, Award No. HRD-124215. Analytical support from Center for Advanced Materials and Smart Structures (CAMS) and JSSN, a member of Southeastern Nanotechnology Infrastructure Corridor (SENIC) and National Nanotechnology Coordinated Infrastructure (NNCI), which is supported by the National Science Foundation (ECCS1542174) is acknowledged. This work was performed in part at the Analytical Instrumentation Facility (AIF) at North Carolina State University, which is supported by the State of North Carolina and the National Science Foundation (award number ECCS-1542015). The AIF is a member of the North Carolina Research Triangle Nanotechnology Network (RTNN), a site in the National Nanotechnology Coordinated Infrastructure (NNCI).

References

[1] J. Divisek, H. F. Oetjen, V. Peinecke, V. M. Schmidt, U. Stimming, Electrochimica Acta 1998, 43, 3811.
[2] N. R. Elezovic, B. M. Babic, P. Ercius, V. R. Radmilovic, L. M. Vracar, N. V. Krstajic, Applied Catalysis B: Environmental 2012, 125, 390.
[3] E. P. Ambrosio, M. A. Dumitrescu, C. Francia, C. Gerbaldi, P. Spinelli, Fuel Cells 2009, 9, 197.
[4] N. Mansor, T. S. Miller, I. Dedigama, A. B. Jorge, J. Jia, V. Bra´zdova´, C. Mattevi, C. Gibbs, D. Hodgson, P. R. Shearing, C. A. Howard, F. Cora`, M. Shaffer, D. J. L. Brett, P. F. McMillan, Electrochimica Acta 2016, 222, 44.
[5] N. Karthikeyan, B. P. Vinayan, M. Rajesh, K. Balaji, A. K. Subramani, S. Ramaprabhu, Fuel Cells 2015, 15, 278.
[6] S. Inagaki, Y. Yokoo, T. Miki, Y. Kubota, Microporous and Mesoporous Materials 2013, 179, 136.
[7] R. K. S. Almeida, J. C. P. Melo, C. Airoldi, Microporous and Mesoporous Materials 2013, 165, 168.
[8] D. Nettelroth, H.-C. Schwarz, N. Burblies, N. Guschanski, P. Behrens, Phys. Status Solidi 2016, 213, 1395.
[9] G. Gupta, D. A. Slanac, P. Kumar, J. D. Wiggins-Camacho, J. Kim, R. Ryoo, K. J. Stevenson, K. P. Johnston, J. Phys. Chem. C 2010, 114, 10796.
[10] D. Zhai, H. Du, B. Li, Y. Zhu, F. Kang, Carbon 2011, 49, 725.
[11] F. J. Maldonado-Ho´dar, C. Moreno-Castilla, J. RiveraUtrilla, Y. Hanzawa, Y. Yamada, Langmuir 2000, 16, 4367. [12] M. Sevilla, A. B. Fuertes, Carbon 2006, 44, 468.
[13] M. Sevilla, C. Sanchı´s, T. Valde´s-Solı´s, E. Morallo´n, A. B. Fuertes, J. Phys. Chem. C 2007, 111, 9749.
[14] M. Sevilla, A. B. Fuertes, Chemical Physics Letters 2010, 490, 63.
[15] M. T. Johnson, K. T. Faber, Journal of Materials Research 2011, 26, 18.
[16] A. Oya, S. Yoshida, J. Alcaniz-Monge, A. Linares-Solano, Carbon 1995, 33, 1085.
[17] M. Yudasaka, K. Tasaka, R. Kikuchi, Y. Ohki, S. Yoshimura, Journal of Applied Physics 1997, 81, 7623.
[18] H. Marsh, D. Crawford, D. W. Taylor, Carbon 1983, 21, 81.
[19] T. Tsubota, Y. Maguchi, S. Kamimura, Journal of Electronic Materials 2015, 44, 4933.
[20] C.-h. Huang, R.-a. Doong, D. Gu, D. Zhao, Carbon 2011, 49, 3055.

[21] J. Tang, T. Wang, X. Sun, Y. Guo, H. Xue, H. Guo, M. Liu, X. Zhang, J. He, Microporous and Mesoporous Materials 2013, 177, 105.
[22] K. N. Sultana, A. L. Fadhel, V. G. Deshmane, S. Ilias, Separation Science and Technology 2018, 53, 1948.
[23] D. Zhao, J. Feng, Q. Huo, N. Melosh, G. H. Fredrickson, B. F. Chmelka, G. D. Stucky, Science 1998, 279, 548.
[24] S. Brunauer, P. H. Emmett, E. Teller, Journal of the American Chemical Society 1938, 60, 309.
[25] M. D. Donohue, G. L. Aranovich, Journal of Colloid and Interface Science 1998, 205, 121.
[26] C. Zhang, X. Zhu, Z. Wang, P. Sun, Y. Ren, J. Zhu, J. Zhu, D. Xiao, Nanoscale Research Letters 2014, 9, 490.
[27] D. Xiang, R. Tang, Q. Su, L. Yin, CrystEngComm 2013, 15, 5442.
[28] T. Jawhari, A. Roid, J. Casado, Carbon 1995, 33, 1561.
[29] A. Ermolieff, A. Chabli, F. Pierre, G. Rolland, D. Rouchon, C. Vannuffel, C. Vergnaud, J. Baylet, M. N. Se´me´ria, Surface and Interface Analysis 2001, 31, 185.
[30] H.-h. Zhou, Q.-l. Peng, Z.-h. Huang, Q. Yu, J.-h. Chen, Y.-f. Kuang, Transactions of Nonferrous Metals Society of China 2011, 21, 581.
[31] Z. Y. Liu, J. L. Zhang, P. T. Yu, J. X. Zhang, R. Makharia, K. L. More, E. A. Stach, Journal of the Electrochemical Society 2010, 157, B906.

